LANGMUIR

pubs.acs.org/Langmuir Article

Constructing Cross-Linked Nanofibrous Scaffold via Dual-Enzyme-Instructed Hierarchical Assembly

Shijin Zhang, William Cortes, and Ye Zhang*

Cite This: https://dx.doi.org/10.1021/acs.langmuir.0c01023 Read Online

ACCESS | Metrics & More | Article Recommendations | Supporting Information

ABSTRACT: To explore the potential of step-by-step assembly in the fabrication of biological materials, we designed and synthesized two peptide-based molecules for enzyme-instructed hierarchical assembly. Upon the treatment of alkaline phosphatase, one molecule undergoes enzyme-instructed self-assembly forming uniformed nanofibers. The other one that can self-assemble into vesicles undergoes enzyme-induced transformation of self-assembly converting vesicles into irregular aggregates upon the treatment of carboxylesterase. Coadministration of two enzymes to a mixture of these two molecules in a stage-by-stage fashion leads to a physically knotted nanofibrous scaffold that is applicable as a nanostructured matrix for cell culture.

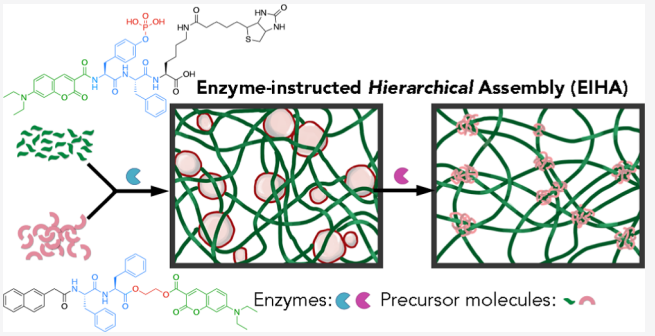

INTRODUCTION

In living systems, advanced biological functions rely on high-level structural complexity.[1] Inspired by biological entities and processes, hierarchical assembly[2,3] is believed to be a promising bottom-up approach of synthetic chemistry to construct materials with tunable advanced structures.[4] In particular, intensive studies on special morphology construction via coordination chemistry[5,6] emphasizing the fluorescence properties[7−11] have been reported. Comparatively, hierarchical assembly is rarely applied in the construction of soft biomaterials. According to theoretical studies on the correspondence between energetics and kinetics for optimal design principles,[12] we decide to program a hierarchical assembly pathway to control the structural energetic stability and kinetic accessibility[3] in stage-by-stage fashion for the fabrication of biomaterials.

Diverse external stimuli have been successfully applied to instruct molecular self-assembly,[13] including chemical stimuli—solvents, acid/base signals, metal ions, gases, biomacromolecules, redox signals, physical stimuli—temperature, magnetic fields, and light. Among stimuli-responsive self-assemblies, enzyme-instructed self-assembly (EISA),[14−19] and enzyme-induced transformation of self-assembly (EITSA),[20] the processes that integrate enzymatic transformation and molecular self-assembly in physiological condition are considered as a practical strategy in biomimetic synthesis of materials.[21] Alkaline phosphatase and carboxylesterase (CES) have been commonly applied in EISA and EITSA because both of them have broad substrate specificity. To confront the challenge of bridging hierarchies of multiple length- and time-scales of self-assembly pathways, these two enzymes with different reaction dynamics are used as external stimuli to instruct the step-by-step assembly.

As demonstrated in Figure 1A, one molecule which undergoes alkaline phosphatase (ALP)-instructed self-assembly forming nanofibrils and the other molecule which undergoes CES-instructed transformation of self-assembled vesicles into nanoaggregates are mixed together in aqueous solution. A stage-by-stage administration of two enzymes in a designated order into the mixture induces coexistence of nanofibrils and vesicles in close contacts followed by the conversion of vesicles into clusters of nanoaggregates and leads to a cross-linked scaffold, which is called enzyme-instructed hierarchical assembly (EIHA).

EXPERIMENTAL SECTION

Materials and Instruments. Fmoc-amino acid, 4-dimethylaminopyridine and 2-chlorotrityl chloride resin were purchased from GL Biochem (Shanghai, China); dimethylformamide (99.5%), dichloromethane (98.0%), *N*,*N*-diisopropylethylamine, trifluoroacetic acid (TFA, 98.0%), *N*-(3-dimethylaminopropyl)-*N*′-ethylcarbodiimide hydrochloride, piperidine (99.0%), Meldrum's acid (98%), methanol (99.0%), ethanol (99.5%), hexane (95.0%) were purchased from Nacalai Tesque Inc., Japan; 2-(1*H*-benzotriazol-1-yl)-1,1,3,3-tetramethyluronium hexafluorophosphate (97.0%) was purchased from Matrix Scientific; *N*,*N*′-diisopropylcarbodiimide (99.0%) was pur-

Received: April 9, 2020
Revised: May 11, 2020
Published: May 17, 2020

https://dx.doi.org/10.1021/acs.langmuir.0c01023
Langmuir XXXX, XXX, XXX−XXX

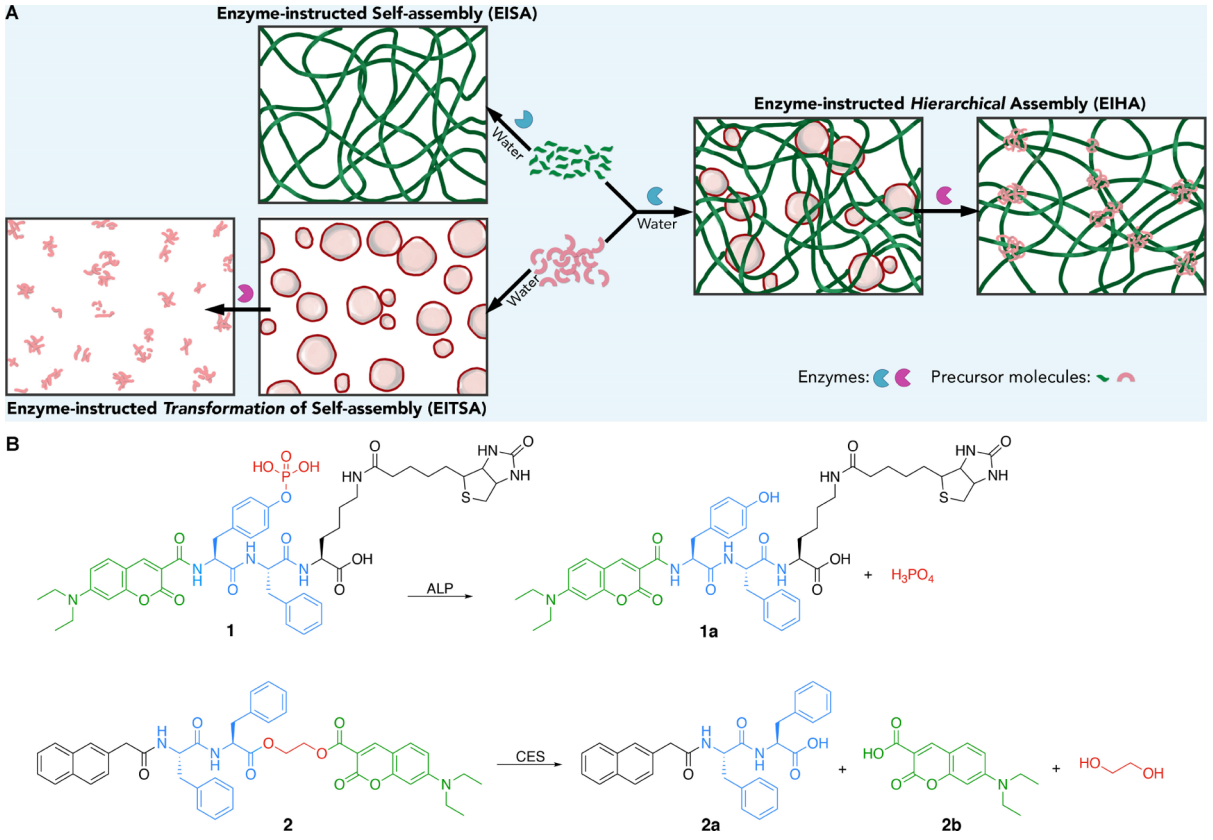

Figure 1. (A) Schematic illustration of constructing physically cross-linked scaffold using EIHA. (B) Chemical structures of peptidic molecules **1** and **2** and their enzymatic catalysis reactions and ALP-catalyzed dephosphorylation of **1** and CES-catalyzed hydrolysis of **2**.

chased from FUJIFILM Wako Pure Chemicals; ethylene glycol (99.8%) was purchased from Sigma-Aldrich. Piperidinium acetate (98.0%), *N*-hydroxysuccinimide (98.0%), and biotin (98.0%) were obtained from Tokyo Chemistry Industry (TCI). 4-(Diethylamino)-salicylaldehyde (98.0%) was purchased from BLD Pharmatech Ltd.; 2-naphthylacetic acid (NapOH, 98.0%) was purchased from Combi-Blocks; organic solvents were dehydrated before the experiment. High performace liquid chromatography (HPLC) purification was performed on an Agilent 1260 Infinity Preparative Pump with Agilent 1260 Infinity Diode Array Detector [eluent: acetonitrile and water (0.1% TFA)]. Mass spectra were recorded using a Thermo LTQ-ETD mass spectrometer (ESI-MS). ^{1}H NMR and ^{13}C NMR spectra were recorded on a JEOL 400 (400 and 101 MHz, respectively) spectrometer.

Synthesis. Synthetic procedures and characterizations of the molecules applied in this study are described in Supporting Information.

Transmission Electron Microscopy Imaging. Sample solution (5 μL) was dropped on the carbon-coated copper grids with enhance hydrophilicity via low discharge for about 1 min. After removing the excess water with filter paper, 5 μL of 1% uranyl acetate was dropped on the grid for about 20 s. After removing the excess solution using a filter paper, the grid was dried in open air. Observation was carried on JEM-1230R with acceleration voltage at 100 kV.

Kinetic Profiling of ALP-Catalyzed Dephosphorylation of 1. Alkaline phosphatase from calf intestine was purchased from Invitrogen (Cat no. 18009-019). Following the instruction, ALP stock solution (1 U/μL) was prepared with the dilution buffer. Stock solutions of compound **1** or mixture of compound **1** and **2** (40 mM in DMSO) were diluted in borate buffer to the desired concentration. Proper volume of ALP stock solution was added into 200 μL of compound solution reaching a final concentration of 1 U. HPLC and liquid chromatography mass spectrometry (LCMS) were applied to identify the reaction products and monitor the progress of hydrolysis at room temperature.

Kinetic Profiling of CES-Catalyzed Hydrolysis of 2. CES from rabbit liver lyophilized powder was purchased from Sigma-Aldrich (E0887-500UN). Following the instruction, CES stock solution (1 U/5 μL) was prepared in borate buffer (pH 8.0). Stock solutions of compound **2** or mixture of compound **1** and **2** (40 mM in DMSO) were diluted in borate buffer to the desired concentration. Proper volume of CES stock solution was added into 200 μL of compound solution reaching a final concentration of 1 U. HPLC and LCMS were applied to identify the reaction products and monitor the progress of hydrolysis at room temperature.

Circular Dichroism Spectroscopy. Circular dichroism (CD) spectra measurements were carried out on a spectrometer JASCO J-820. The bandwidth was set at 1.0 nm and the measurement range was 190−400 nm. All measurements were carried out in a 1 mm quartz cuvette at room temperature. Theoretical curve was obtained by a simple sum of every single components.

Rheological Measurement. Rheology tests were conducted on Anton Paar MCR302; parallel-plate geometry with an upper plate diameter of 25 mm was used during the experiment, and the gap was 0.1 mm. Throughout the experiment, the stage temperature was maintained at 25 °C. The specimen was transferred to the stage by spatula, dynamic strain (0.1−100%) was performed at 6.28 rad/s, maximum storage moduli in the linear range of the strain sweep test was selected for frequency sweep test (0.1−200 rad/s).

Cell Viability Assay. HeLa cells in exponential growth phase were seeded in a 96 well plate at a concentration of 8000 cells/well for all cell lines. The cells were allowed to attach to the wells for 12 h at 37 °C, 5% CO_2. The culture medium was removed followed by addition of 100 μL culture medium containing different concentrations (50, 100, 200, 500, and 1000 μM) of compound 1 and 2. After the desired time of incubation, 10 μL MTT solution (5 mg/mL) was added to each well and incubated at 37 °C for another 4 h, and then, 100 μL of

https://dx.doi.org/10.1021/acs.langmuir.0c01023
Langmuir XXXX, XXX, XXX−XXX

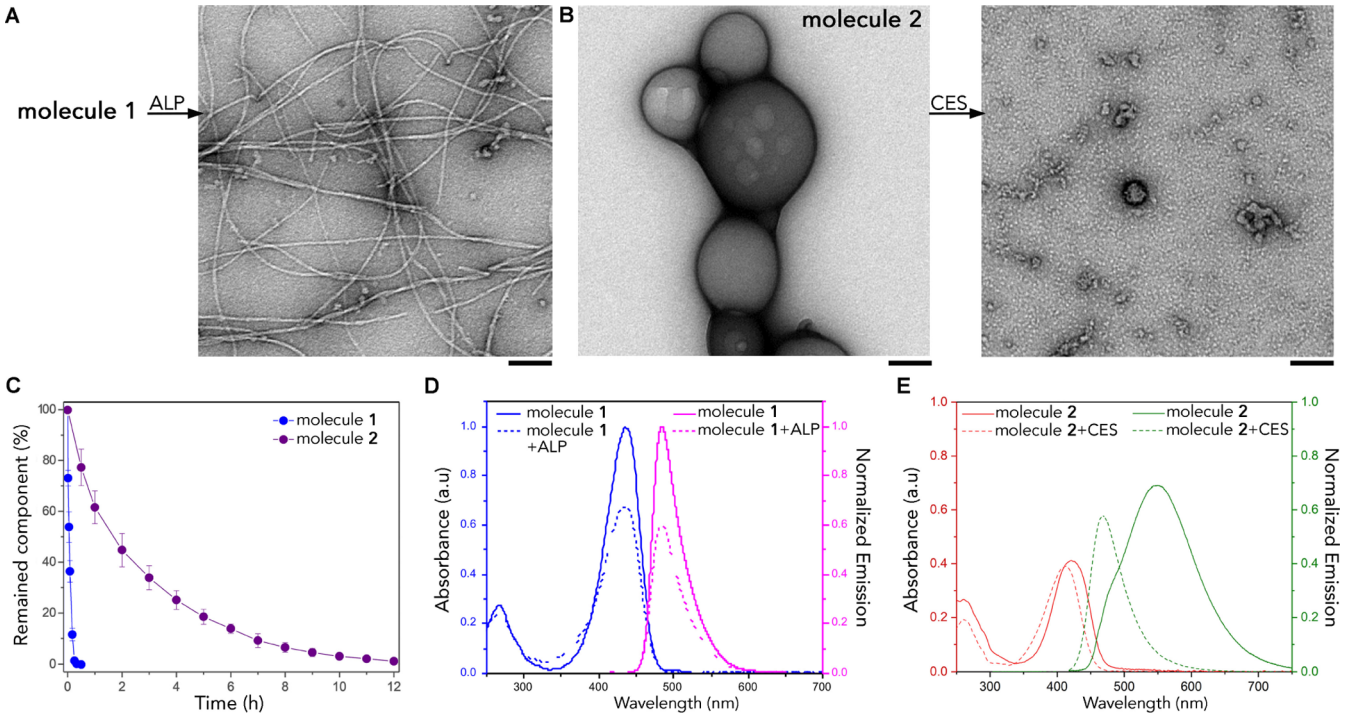

Figure 2. (A) TEM images of ALP-catalyzed dephosphorylation of molecule **1** (1 mM) induced self-assembly. Scale bar represents 100 nm. (B) TEM images of CES-catalyzed hydrolysis of molecule **2** (1 mM) induced transformation of self-assembly. Scale bars represent 100 nm. (C) Kinetic profiles of ALP-catalyzed dephosphorylation of molecule **1**, and CES-catalyzed hydrolysis of molecule **2** separately in borate buffer at 25 °C. (D) UV−vis absorption spectra and emission spectra (excited at 405 nm) of molecule **1** (0.2 mM) in borate buffer at 25 °C before and after treatment with ALP (1 U/mL) for 12 h. (E) UV−vis absorption spectra and emission spectra (excited at 405 nm) of molecule **2** (0.2 mM) in borate buffer at 25 °C before and after treatment with CES (0.2 U/mL) for 12 h.

sodium docedyl sulfate (SDS) solution (10% in Milli-Q water) was added to stop the reduction reaction and dissolve the purple formazan. The absorbance at 570 nm was measured using a Nivo 3 microplate reader (PerkinElmer). All experiments were performed in triplicate and repeated three times.

Multicellular Spheroid Culture Assay. To introduce various nanostructures into the culture medium, we first prepared the culture medium containing both molecule **1** (200 μM) and molecule **2** (200 μM). And then the enzymes were introduced to the solutions in different orders. For spheroid formation, a fixed number of HeLa cells (2000) was seeded in 100 μL of complete culture medium (with and without the nanostructures) in round bottomed, ultra-low attachment 96-well plates (Thermo Scientific, 174929 96U bottom plate) and incubated for 72 h. For each culture condition, a minimum of three independent repeat experiments was performed ($n \geq 3$). The growth of spheroids was recorded using IncuCyte S3.

RESULTS AND DISCUSSION

Molecular Design and Synthesis. Regarding the broad impact of peptide-based scaffolds in biomedical applications,[22−25] two peptidic molecules **1** and **2** are designed as precursors for EIHA. As shown in Figure 1B, 7-(diethyamino)-coumarin-3-carboxylic acid[26,27] that is predominantly used as a biomedical inhibitor is applied as the aromatic building block facilitating intermolecular $\pi-\pi$ stacking for both molecules. Based on the instructions of previous design on EISA induced nanofibril formation, by coupling the aromatic building block to the N-terminal of Tyr(PO_3H_2)-Phe-Lys(biotin), we obtained hydrophilic molecule **1**. The phosphor-tyrosine unit of molecule **1** response to enzyme leading to ALP-catalyzed dephosphorylation. Coupling biotin to the side chain of lysine is to enhance the molecular interaction with cell surface via biotin−avidin binding.[28,29] Upon the treatment of ALP, molecule **1** will transform into relatively hydrophobic derivative **1a** triggering molecular self-assembly. To have self-assembled vesicles,[20] molecule **2** was synthesized by linking naphthalene-Phe-Phe, the classic peptide building block for $\pi-\pi$ interaction and hydrogen bonding oriented self-assembly, to 7-(diethyamino)-coumarin-3-carboxylic acid via ethylene glycol. Upon the treatment of CES, molecule **2** is hydrolyzed into the self-assembly building block **2a** and the aromatic building block **2b**.

EISA of Molecule 1 and EITSA of Molecule 2. Molecule **1** is highly soluble in water. Upon the treatment of ALP, dephosphorylation of molecule **1** to **1a** triggers molecular self-assembly forming uniform nanofibrils (Figure 2A). Different from that, molecule **2** self-assembles in borate buffer forming vesicles with a broad range of diameters. Upon the treatment of CES, hydrolysis of **2** to **2a** and **2b** triggers disassembly of vesicles into clusters of nanoaggregates in irregular shapes (Figure 2B).

The kinetic profiles of both catalytic reactions under a single component condition were recorded (Figure 2C). At room temperature (25 °C), ALP-catalyzed dephosphorylation of molecule **1** into **1a** is completed within half an hour (Figure S1), which is more than 20 times faster than the CES-catalyzed hydrolysis of **2** into **2a** and **2b** that takes about 12 h (Figure S2). Consequently, the formation of nanofibrils via EISA is much faster than the disassembly of vesicles into nanoaggregates via EITSA. Regarding the blue fluorescence of aromatic building block **2b** shared by both molecules, the absorption and emission spectra of molecules **1** and **2** before and after the catalytic reactions were characterized. For molecule **1** in borate buffer, the absorption and emission

https://dx.doi.org/10.1021/acs.langmuir.0c01023
Langmuir XXXX, XXX, XXX−XXX

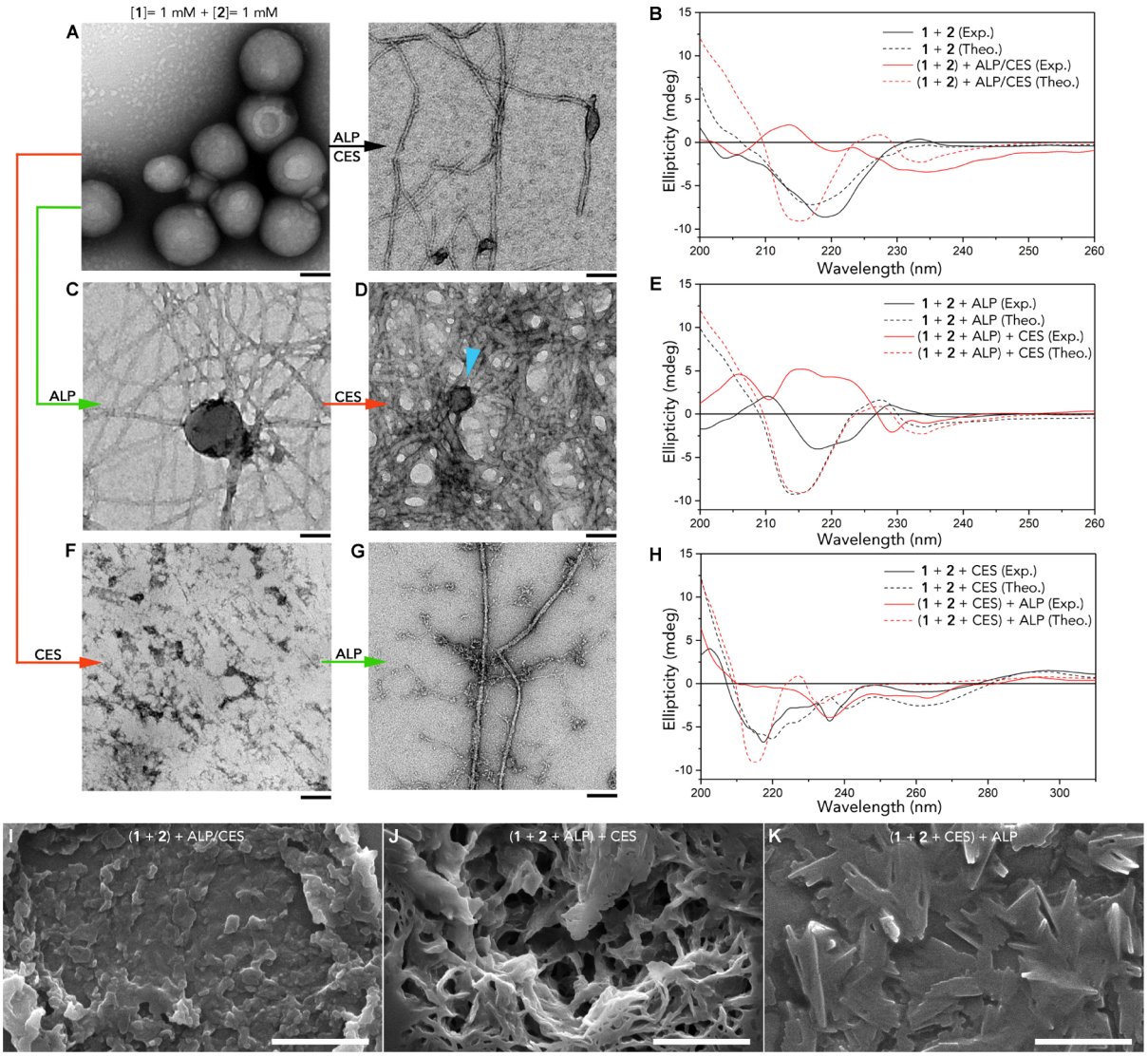

Figure 3. TEM images of molecule **1** (1 mM) and molecule **2** (1 mM) mixture in borate buffer at 25 °C before and after treatment with ALP and CES simultaneously for 16 h (A), treated with ALP for 30 min (C) first, and then with CES for 14 h (D) and treated first with CES for 12 h (F) and then with ALP for 40 min (G). Scale bars represent 100 nm. (B) CD spectra of molecule **1** and molecule **2** mixture in borate buffer at 25 °C before and after treated by ALP and CES simultaneously. (E) CD spectra of molecule **1** and molecule **2** mixture in borate buffer at 25 °C treated by ALP for 30 min, and after the second stage treatment with CES. (H) CD spectra of molecule **1** and molecule **2** mixture in borate buffer at 25 °C treated by CES for 12 h, and after the second stage treatment with ALP. Solid and dash lines in panels (B,E,H) represent experimental (Exp.) and theoretical (Theo.) CD spectra, respectively. SEM image of end stage of molecule **1** (1 mM) and molecule **2** (1 mM) mixture in borate buffer at 25 °C treated with ALP and CES simultaneously (I), treated first with ALP for 30 min and then with CES for 14 h (J) and treated first with CES for 12 h and then with ALP for 40 min (K). The scale bars of panel (I–K) represent 2 μm.

peaks remain at 434 and 484 nm, respectively, before and after the ALP-catalyzed dephosphorylation (Figure 2D), while both intensities decrease after EISA because of self-assembly shielding effect.[30]olecule **2** in borate buffer has an absorption peak at 421 nm and a fluorescent peak at 546 nm. After the treatment with CES, the absorption peak shifts to 412 nm, and the fluorescent peak shifts to 468 nm (Figure 2E). Compare to the absorption and emission spectra of **2b** that have peaks at 424 and 472 nm (Figure S3), respectively, CES-induced EITSA causes blue shifts via both morphological change and component change.

Stage-By-Stage Administration of Enzymes to the Mixture of 1 and 2 Leads to EIHA. Similar as the self-assembly of molecule **2** in borate buffer, the 1:1 mixture of molecules **1** and **2** at the same total concentration forms vesicles of a wide range of diameters (Figure 3A). The CD spectrum of the mixture is similar to the simple sum of both single-component spectra. Considering the solubility of molecule **1**, the addition of molecule **1** may induce alteration of the solution environment of molecule **2** slightly affecting its self-assembly instead of inducing coassembly with molecule **2** (Figure 3B). The administration of two enzymes to the mixture in different orders leads to distinct nanostructures. For example, the coadministration of ALP and CES simultaneously to the mixture of two molecules leads to scattered beaded nanofibrils (Figure 3A right panel) via molecular coassembly confirmed by the CD spectrum which is distinct from the theoretical calculation – the sum of CD spectra of **1a**, **2a**, and **2b** (Figure 3B), while the administration of two enzymes in an order of ALP first and CES second triggers the formation of

https://dx.doi.org/10.1021/acs.langmuir.0c01023
Langmuir XXXX, XXX, XXX–XXX

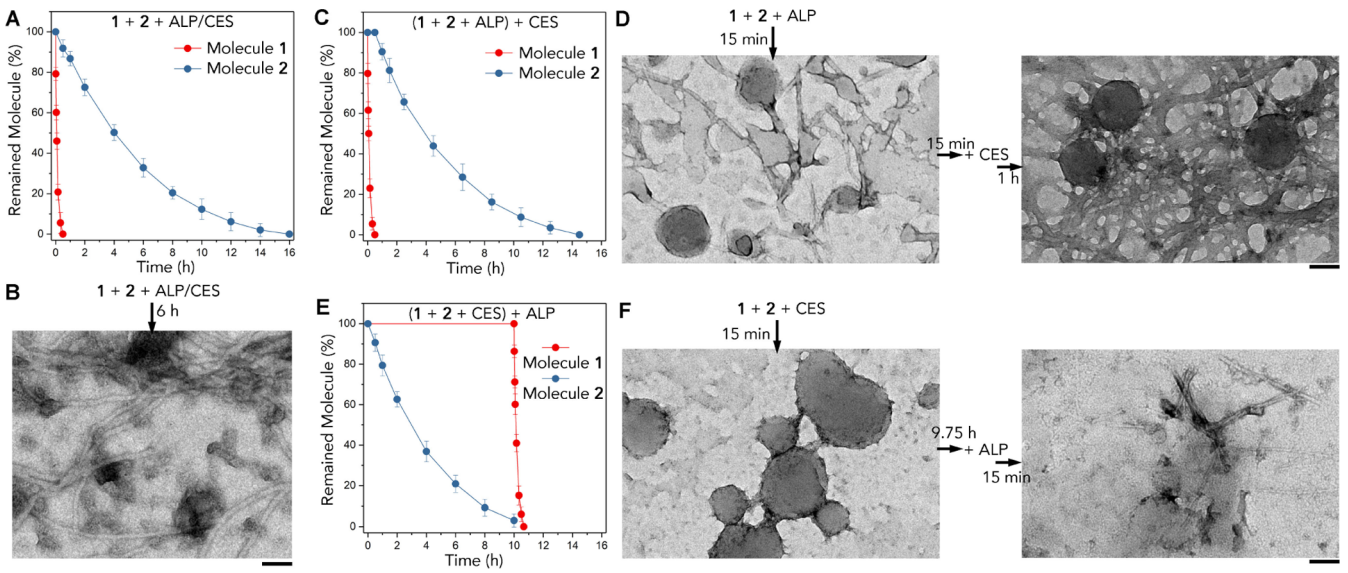

Figure 4. (A) Kinetic profiles of ALP-catalyzed hydrolysis of **1** and CES-catalyzed hydrolysis of **2**, when ALP and CES are added into the mixture of **1** and **2** simultaneously. (B) TEM image of **1** and **2** mixture reacting with ALP and CES simultaneously for 6 h. Scale bar represents 100 nm. (C) Kinetic profiles of ALP-catalyzed hydrolysis of **1** and CES-catalyzed hydrolysis of **2** when **1** and **2** mixture reacts with ALP first and then CES. (D) TEM image of **1** and **2** mixture reacting with ALP for 15 min, and TEM image of **1** and **2** mixture first reacting with ALP for 30 min and then with CES for 1 h. Scale bar represents 100 nm. (E) Kinetic profiles of ALP-catalyzed hydrolysis of **1** and CES-catalyzed hydrolysis of **2** when **1** and **2** mixture reacts with CES first, then ALP. (F) TEM image of **1** and **2** mixture reacting with CES for 15 min, and TEM image of **1** and **2** mixture first reacting with CES for 10 h and then with ALP for 15 min. Scale bar represents 100 nm.

uniform nanofibrils around vesicles in close contacts (Figure 3C) first, and then, the transition of vesicles into clusters crosslinking the nanofibrous into scaffold (Figure 3D indicated by blue arrow head) via coassembly confirmed by the comparisons between the experimental and theoretical CD spectra (Figure 3E). Distinct from that, the administration of two enzymes in an order of CES first and ALP second induces the disassembly of vesicles into scattered irregular aggregates first (Figure 3F) and then the formation of nanofibrils tangling with irregular nanoaggregates (Figure 3G) via coassembly, which is also confirmed the CD spectra comparisons (Figure 3H). Consistent with the morphology difference induced by three enzyme administration orders, the CD spectra of final nanostructures are distinct from each other. Scanning electron microscopy (SEM) revealed the difference of final structures in macroscopic scale. As shown in Figure 3I, coadministration of the two enzymes simultaneously into the mixture of two molecules leads to piles of aggregates. Administration of enzymes in the order of ALP then CES leads to fibrous scaffolds (Figure 3J), and the administration of CES first then ALP leads to plies of short sticks (Figure 3K).

Dynamics and Transitional Morphology Study of Stage-By-Stage Assembly. By comparing the kinetics of ALP-catalyzed dephosphorylation of molecule **1** and CES-catalyzed hydrolysis of molecule **2** in three different enzyme-administration processes and the correlated transmission electron microscopy (TEM) characterizations of molecular assembly at transition stages, we try to explore the general implications underlying the stage-by-stage hierarchical assembly. During the coadministration of both enzymes simultaneously to the mixture of molecules **1** and **2**, ALP-catalyzed dephosphorylation of molecule **1** remains as the same reaction speed as during the administration of ALP solely in molecule **1**, while the CES-catalyzed hydrolysis of molecule **2** was slowed down by requiring 4 more hours to complete the reaction that takes 12 h in a single component condition (Figure 4A). In the middle of the reaction when ALP-catalyzed dephosphorylation is completed but CES-catalyzed hydrolysis is still ongoing, there is a surface interaction among **1a**-assembled-nanofibers, **2**-assembled-vesicles, and disassembled vesicles. TEM imaging reveals consistent results that nanoaggregates and deformed vesicles attach to nanofibrils (Figure 4B). Besides the "solid effect" induced by the nanofibrils formation, the physical interactions between the different nanofilaments may also slow down the CES-catalyzed hydrolysis, and scattered beaded nanofibrils are formed in the end of the process.

During stage-by-stage administration of two enzymes in the order of ALP and CES, ALP-catalyzed dephosphorylation of molecule **1** remains as the same reaction speed as during the administration of ALP solely in molecule **1**, while the CES-catalyzed hydrolysis of molecule **2** required about 14 h, which is 2 h slower than the single component condition, but 2 h faster than the coadministration process (Figure 4C). During the first stage enzyme administration, the TEM image reveals short nanofibrils forming around scattered vesicles. One hour after the second stage enzyme administration, TEM imaging reveals dense nanofibrils tangling around vesicles with close surface contacts. The two TEM images confirm that the formation of nanofibers induced by ALP-catalyzed dephosphorylation does not affect the morphology of **2**-assembled-vesicles. The second stage EITSA under the condition of close surface interactions between nanofibers and vesicles leads to the formation of dense nanofibrous scaffold tied up by the nanoaggregates (Figure 4D). During stage-by-stage administration of two enzymes in the order of CES and ALP, the CES-catalyzed hydrolysis of **2** sped up to complete the reaction in 10 h suggesting that the hydrophilic molecule **1** may moderate the "solid effect" induced by assembled vesicles, while the following ALP-catalyzed hydrolysis of **1** remained the same speed as in single component condition (Figure 4E).

https://dx.doi.org/10.1021/acs.langmuir.0c01023
Langmuir XXXX, XXX, XXX−XXX

Shortly after the first stage enzyme administration, TEM images showed vesicles with rough edges and disrupt shapes indicating the initiation of disassembly. Shortly after the second stage of enzyme administration, the TEM image reveals the formation of short nanofibrils surrounded by irregular nanoaggregates, which eventually leads to elongated nanofibrils with attached nanoaggregates (Figure 4F). Comparing these three enzyme-administration processes, we found that the coexistence of nanofibrils and nanovesicles in close contacts prior to the second stage of assembly is critical to scaffold formation. Disassembling these well inserted vesicles can physically knot the nanofibrils together by transformed nanoaggregates, and the stage-by-stage administration successfully controls the interface interactions among various assembled nanostructures leading to distinct hierarchical morphologies that are confirmed by TEM imaging and CD characterization.

Multicellular Spheroid Culture in Stage-By-Stage Assembled Nanostructures. The mechanical properties of the final nanostructures obtained via three pathways were evaluated via rheology measurements. The oscillatory frequency sweep (Figure 5A) confirms that the nanostructures

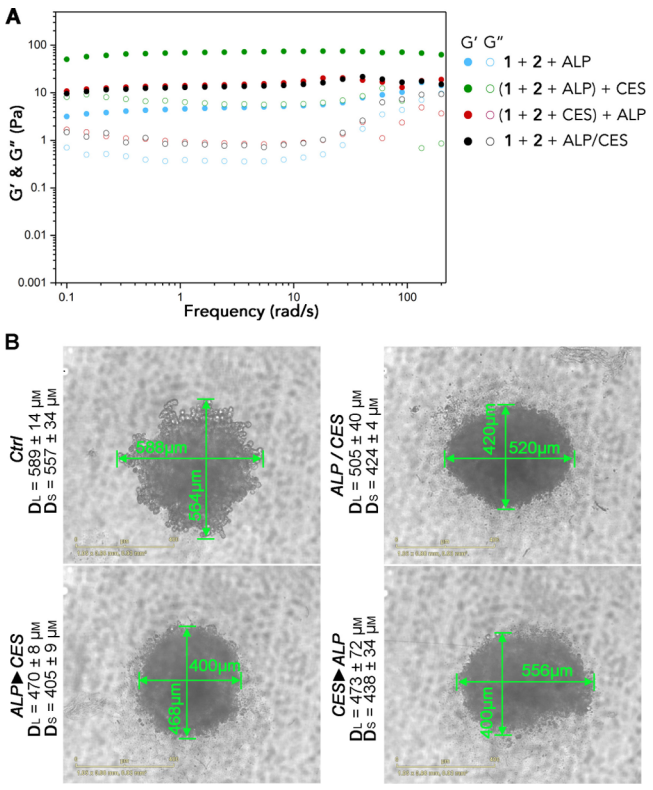

Figure 5. (A) The frequency sweep tests of coassembled nanostructures obtained by administration of two enzymes in three different orders. (B) Optical images of HeLa cell spheroids cultured under various conditions exhibiting the influence of nanostructures obtained by stage-by-stage assembly.

obtained via stage-by-stage administration of ALP; then, CES to the mixture of **1** and **2** is much stronger than the nanostructures obtained via other pathways, which is consistent with the TEM image of physically cross-linked nanofibrous scaffold.

Various three-dimensional (3D) matrices have been applied[31−33] in cancer spheroid culture to adjust 3D cell−cell contacts to resemble the physiological microenvironments of different solid tumors for cancer research.[34] Regarding the biocompatibility of both molecules **1** and **2** (Figure S4), the nanostructures obtained via various pathways are applied in multicellular spheroid culture. By examining the diameters of the spheroids cultured from the same number of HeLa cells, we found that tightly packed spheroids were obtained upon the treatment of nanostructures compare to the control condition (Figure 5B) due to the cell−nanostructure interaction via biotin−avidin binding. By summarizing the length of long diameter and short diameter of spheroids cultured in various nanostructures, we also found that the crosslinked scaffold obtained via stage-by-stage treatment of ALP and CES facilitated the growth of the most tightly packed spheroids with less variations. Besides the accurate size control of cancer spheroids, adjusting spheroid packing density via synthetic matrix will also facilitate the tumor cell microenvironment mimicking that both are potentially helpful to the drug screening.

CONCLUSIONS

We introduced here the construction of a variable assembly system guided by two enzymes, ALP and CES. The alteration of enzyme administration orders leads to distinct nanostructures, and a stage-by-stage administration of ALP and CES leads to hierarchical assembly forming physically cross-linked nanofibrous scaffold which is potentially applicable in the control of 3D cell−cell contacts in multicellular spheroid culture. Besides that, the underlining mechanism studies also reveal that at defined temperature and concentration, the ALP-catalyzed dephosphorylation is barely affected by the surrounding nanostructures, while the CES-catalyzed hydrolysis of **2** is affected by the surrounding molecules and nanostructures. By regulating the enzyme administration order, the hydrolysis reaction speed is altered which influences the formation and distribution of various nanofilaments leading to prospective hierarchical assembly. By demonstrating such practical design of step-by-step assembly for constructing nanostructured soft material, it is proved that hierarchical assembly offers promising potentials to the engineering of synthetic extracellular matrix (ECM). Advanced extension of this design is programmed assembly of multiple functional peptides for fine adjustment of cell−cell and cell−ECM interactions.

ASSOCIATED CONTENT

Supporting Information

The Supporting Information is available free of charge at https://pubs.acs.org/doi/10.1021/acs.langmuir.0c01023.

Synthesis and characterization of molecules, UV−vis absorption and emission measurements, and cell viabilities (PDF)

AUTHOR INFORMATION

Corresponding Author

Ye Zhang − *Bioinspired Soft Matter Unit, Okinawa Institute of Science and Technology Graduate University, Okinawa 904-0495, Japan;* orcid.org/0000-0001-7433-1820; Email: ye.zhang@oist.jp

https://dx.doi.org/10.1021/acs.langmuir.0c01023
Langmuir XXXX, XXX, XXX−XXX

Authors

Shijin Zhang − *Bioinspired Soft Matter Unit, Okinawa Institute of Science and Technology Graduate University, Okinawa 904-0495, Japan*

William Cortes − *Bioinspired Soft Matter Unit, Okinawa Institute of Science and Technology Graduate University, Okinawa 904-0495, Japan*

Complete contact information is available at: https://pubs.acs.org/10.1021/acs.langmuir.0c01023

Notes

The authors declare no competing financial interest.

■ ACKNOWLEDGMENTS

This work was supported by the Proof-of-Concept program of OIST, Okinawa Institute of Science and Technology Graduate University (OIST), and Takeda Science Foundation.

■ REFERENCES

(1) Wolf, Y. I.; Katsnelson, M. I.; Koonin, E. V. Physical foundations of biological complexity. *Proc. Natl. Acad. Sci. U.S.A.* **2018**, *115*, E8678−E8687.

(2) Gerbelli, B. B.; Vassiliades, S. V.; Rojas, J. E. U.; Pelin, J. N. B. D.; Mancini, R. S. N.; Pereira, W. S. G.; Aguilar, A. M.; Venanzi, M.; Cavalieri, F.; Giuntini, F.; Alves, W. A. Hierarchical Self-Assembly of Peptides and its Applications in Bionanotechnology. *Macromol. Chem. Phys.* **2019**, *220*, 1900085.

(3) Whitelam, S. Hierarchical assembly may be a way to make large information-rich structures. *Soft Matter* **2015**, *11*, 8225−8235.

(4) Chen, L.-J.; Yang, H.-B. Construction of Stimuli-Responsive Functional Materials via Hierarchical Self-Assembly Involving Coordination Interactions. *Acc. Chem. Res.* **2018**, *51*, 2699−2710.

(5) Amabilino, D. B.; Ashton, P. R.; Boyd, S. E.; Lee, J. Y.; Menzer, S.; Stoddart, J. F.; Williams, D. J. The five-stage self-assembly of a branched heptacatenane. *Angew. Chem. Int. Ed. Engl.* **1997**, *36*, 2070−2072.

(6) Huo, G.-F.; Shi, X.; Tu, Q.; Hu, Y.-X.; Wu, G.-Y.; Yin, G.-Q.; Li, X.; Xu, L.; Ding, H.-M.; Yang, H.-B. Radical-Induced Hierarchical Self-Assembly Involving Supramolecular Coordination Complexes in Both Solution and Solid States. *J. Am. Chem. Soc.* **2019**, *141*, 16014−16023.

(7) Peng, H.-Q.; Liu, B.; Wei, P.; Zhang, P.; Zhang, H.; Zhang, J.; Li, K.; Li, Y.; Cheng, Y.; Lam, J. W. Y.; Zhang, W.; Lee, C.-S.; Tang, B. Z. Visualizing the Initial Step of Self-Assembly and the Phase Transition by Stereogenic Amphiphiles with Aggregation-Induced Emission. *ACS Nano* **2019**, *13*, 839−846.

(8) Qiu, H.; Hudson, Z. M.; Winnik, M. A.; Manners, I. Multidimensional hierarchical self-assembly of amphiphilic cylindrical block comicelles. *Science* **2015**, *347*, 1329−1332.

(9) Shao, L.; Sun, J.; Hua, B.; Huang, F. An AIEE fluorescent supramolecular cross-linked polymer network based on pillar[5]arene host-guest recognition: construction and application in explosive detection. *Chem. Commun.* **2018**, *54*, 4866−4869.

(10) Yan, X.; Li, S.; Cook, T. R.; Ji, X.; Yao, Y.; Pollock, J. B.; Shi, Y.; Yu, G.; Li, J.; Huang, F.; Stang, P. J. Hierarchical Self-Assembly: Well-Defined Supramolecular Nanostructures and Metallohydrogels via Amphiphilic Discrete Organoplatinum(II) Metallacycles. *J. Am. Chem. Soc.* **2013**, *135*, 14036−14039.

(11) Zhuo, M. P.; Wu, J. J.; Wang, X. D.; Tao, Y. C.; Yuan, Y.; Liao, L. S. Hierarchical self-assembly of organic heterostructure nanowires. *Nat. Commun.* **2019**, *10*, 3839.

(12) Morphew, D.; Chakrabarti, D. Programming hierarchical self-assembly of colloids: matching stability and accessibility. *Nanoscale* **2018**, *10*, 13875−13882.

(13) Menger, F. M. Supramolecular chemistry and self-assembly. *Proc. Natl. Acad. Sci. U.S.A.* **2002**, *99*, 4818−4822.

(14) Feng, Z.; Han, X.; Wang, H.; Tang, T.; Xu, B. Enzyme-Instructed Peptide Assemblies Selectively Inhibit Bone Tumors. *Chem* **2019**, *5*, 2442−2449.

(15) Li, G.; Sasaki, T.; Asahina, S.; Roy, M. C.; Mochizuki, T.; Koizumi, K.; Zhang, Y. Patching of Lipid Rafts by Molecular Self-Assembled Nanofibrils Suppresses Cancer Cell Migration. *Chem* **2017**, *2*, 283−298.

(16) Feng, Z.; Wang, H.; Chen, X.; Xu, B. Self-Assembling Ability Determines the Activity of Enzyme-Instructed Self-Assembly for Inhibiting Cancer Cells. *J. Am. Chem. Soc.* **2017**, *139*, 15377−15384.

(17) Wang, H.; Feng, Z.; Xu, B. Bioinspired assembly of small molecules in cell milieu. *Chem. Soc. Rev.* **2017**, *46*, 2421−2436.

(18) Zhou, J.; Du, X.; Berciu, C.; He, H.; Shi, J.; Nicastro, D.; Xu, B. Enzyme-Instructed Self-Assembly for Spatiotemporal Profiling of the Activities of Alkaline Phosphatases on Live Cells. *Chem* **2016**, *1*, 246−263.

(19) Zhou, J.; Du, X.; Yamagata, N.; Xu, B. Enzyme-Instructed Self-Assembly of Small D-Peptides as a Multiple-Step Process for Selectively Killing Cancer Cells. *J. Am. Chem. Soc.* **2016**, *138*, 3813−3823.

(20) Zhang, S.; Hu, X.; Mang, D.; Sasaki, T.; Zhang, Y. Self-delivery of N-hydroxylethyl peptide assemblies to the cytosol inducing endoplasmic reticulum dilation in cancer cells. *Chem. Commun.* **2019**, *55*, 7474−7477.

(21) Du, X.; Zhou, J.; Shi, J.; Xu, B. Supramolecular Hydrogelators and Hydrogels: From Soft Matter to Molecular Biomaterials. *Chem. Rev.* **2015**, *115*, 13165−13307.

(22) Matson, J. B.; Stupp, S. I. Self-assembling peptide scaffolds for regenerative medicine. *Chem. Commun.* **2012**, *48*, 26−33.

(23) Fukunaga, K.; Tsutsumi, H.; Mihara, H. Self-Assembling Peptides as Building Blocks of Functional Materials for Biomedical Applications. *Bull. Chem. Soc. Jpn.* **2019**, *92*, 391−399.

(24) Li, J.; Xing, R.; Bai, S.; Yan, X. Recent advances of self-assembling peptide-based hydrogels for biomedical applications. *Soft Matter* **2019**, *15*, 1704−1715.

(25) Zhao, L.; Zou, Q.; Yan, X. Self-Assembling Peptide-Based Nanoarchitectonics. *Bull. Chem. Soc. Jpn.* **2019**, *92*, 70−79.

(26) Lin, Q.; Bao, C.; Fan, G.; Cheng, S.; Liu, H.; Liu, Z.; Zhu, L. 7-Amino coumarin based fluorescent phototriggers coupled with nano/bio-conjugated bonds: Synthesis, labeling and photorelease. *J. Mater. Chem.* **2012**, *22*, 6680−6688.

(27) Liu, X.; Cole, J. M.; Chow, P. C. Y.; Zhang, L.; Tan, Y.; Zhao, T. Dye Aggregation and Complex Formation Effects in 7-(Diethylamino)-coumarin-3-carboxylic Acid. *J. Phys. Chem. C* **2014**, *118*, 13042−13051.

(28) Anamelechi, C. C.; Clermont, E. E.; Brown, M. A.; Truskey, G. A.; Reichert, W. M. Streptavidin binding and endothelial cell adhesion to biotinylated fibronectin. *Langmuir* **2007**, *23*, 12583−12588.

(29) Dou, X.-Q.; Zhang, J.; Feng, C. Biotin-Avidin Based Universal Cell-Matrix Interaction for Promoting Three-Dimensional Cell Adhesion. *ACS Appl. Mater. Interfaces* **2015**, *7*, 20786−20792.

(30) Nishizawa, S.; Kato, Y.; Teramae, N. Fluorescence sensing of anions via intramolecular excimer formation in a pyrophosphate-induced self-assembly of a pyrene-functionalized guanidinium receptor. *J. Am. Chem. Soc.* **1999**, *121*, 9463−9464.

(31) Dou, X.-Q.; Feng, C.-L. Amino Acids and Peptide-Based Supramolecular Hydrogels for Three-Dimensional Cell Culture. *Adv. Mater.* **2017**, *29*, 1604062.

(32) Dou, X.; Mehwish, N.; Zhao, C.; Liu, J.; Xing, C.; Feng, C. Supramolecular Hydrogels with Tunable Chirality for Promising Biomedical Applications. *Acc. Chem. Res.* **2020**, *53*, 852−862.

(33) Tam, R. Y.; Smith, L. J.; Shoichet, M. S. Engineering Cellular Microenvironments with Photo- and Enzymatically Responsive Hydrogels: Toward Biomimetic 3D Cell Culture Models. *Acc. Chem. Res.* **2017**, *50*, 703−713.

(34) Nath, S.; Devi, G. R. Three-dimensional culture systems in cancer research: Focus on tumor spheroid model. *Pharmacol. Ther.* **2016**, *163*, 94−108.

https://dx.doi.org/10.1021/acs.langmuir.0c01023
Langmuir XXXX, XXX, XXX−XXX